FACTOR ANALYSIS OF SCINTIGRAPHIC IMAGE SEQUENCES WITH INTEGRATED CONVOLUTION MODEL OF FACTOR CURVES

Václav Šmídl, Ondřej Tichý,
Department of Adaptive Systems
Institute of Information Theory and Automation
Prague, Czech Republic,
email: {smidl,otichy}@utia.cas.cz

Martin Šámal
Department of Nuclear Medicine,
1st Faculty of Medicine,
Charles University Prague,
Czech Republic

ABSTRACT
Factor analysis and deconvolution are commonly used tools in analysis of time activity analysis of biological organs in scintigraphic data. Typically, these are used independently such that the output of the former is taken as an input to the latter. Each method is thus unaware of the restrictions imposed by the other and fails to respect them. In this paper, we propose a probabilistic model that integrates convolution into the factor analysis model. We develop an approximate Bayesian estimation of the model parameters based on Variational Bayes approximation. The new variant of the factor analysis model is suitable for modeling of a range of biological processes where convolution kernels are known to have restricted shapes. Properties of the new model are illustrated on analysis of data from dynamic renal scintigraphy. The proposed model provides more realistic estimates of the convolution kernels.

KEY WORDS
Factor Analysis, Blind deconvolution, Scintigraphy, Medical Image Sequence

1 Introduction

Analysis of a dynamic scintigraphy data is typically performed in two steps. In the first step, image components and their time activity curves are extracted, and the time activity curves are analyzed for diagnostic information in the second step. Quite often, models and assumptions used in one step are different from those in the second step. For example, in functional analysis of renal studies, the image components and time activity curves may be extracted by factor analysis [1] or regions-of-interest, while the diagnostic information is processed by deconvolution [5]. Since the assumptions of these two methods differ, proper combination of these two steps must be supervised by an expert who is capable of correcting the mismatch. This skill is difficult to transfer without extensive training. Our long term objective is to build more advanced mathematical model that will incorporate as much of the expert knowledge as possible. As a step in this direction, we propose a model that incorporates convolution parametrization of the factor curves into the model of factor analysis.

Factor analysis is a classical statistical method that has been used in analysis of medical image sequences in scintigraphy [1], ultrasound [7] and PET [4]. A common problem of the factor analysis model is that the basic unconstrained model allows for infinitely many solutions. Further restrictions on the factors has to be imposed to obtain physiologically meaningful solution. Typical restrictions are positivity of the curves [11]. However, positivity alone does not guarantee neither biological meaningful curves, nor uniqueness of decomposition. Uniqueness is assured only when all factor images contain at least one pixel at which all other images have zero activity [12]. This condition does not hold e.g. in renal scintigraphy, where activity of the background tissue is present in all pixels. Additional constraints are necessary to restrict the space of possible solutions. One such extra constraint is specific shape of convolution kernels of the factor curves. This knowledge is well known in the second step of the analysis using deconvolution [5, 2].

Combination of these assumption in one model results in rather complex model without an analytical solution. The Variational Bayes methodology has been successfully used for approximate solution of closely related models of independent component analysis [8], variants of factor analysis [10], and convolution models with unknown kernels and input functions [9]. The Variational Bayes is computationally less demanding than popular Monte Carlo techniques. However, solution of the presented model is significantly more demanding than solution of the previous models.

2 Background

To illustrate relation of the variational Bayes solution to previously known methods, we briefly review variational factor analysis and deconvolution with monotonic kernels.

2.1 Variational Factor Analysis (FA)

The task is to analyze a sequence of n images obtained by scintigraphic camera in time $t = 1, \ldots, n$. Every image consists of p pixels. These are aggregated in a matrix of measurement, $D \in \mathbf{R}^{p \times n}$, which consists of p-dimensional vectors in each column, one for each time of observation. We

assume that each image in the sequence is formed from r factor images by linear combination, typically $r < n \ll p$. Matrix $A \in \mathbf{R}^{p\times r}$ is composed from the factor images, one image in each column. Every factor image has its associated time-activity curve, $x_j = [x_{1,j},\ldots,x_{n,j}]$, that are stored as columns of time-activity matrix $X \in \mathbf{R}^{n\times r}$. Both matrices A and X are unknown and we seek their estimates.

The model can be written in the following matrix form

$$D = AX' + E \tag{1}$$

where $E \in \mathbf{R}^{p\times n}$ is the matrix of noise. Matrix D is composed of measurements of radioactive particles which are known to have Poisson distribution. An appropriate covariance matrix of errors E can be found using correspondence analysis [3]:

$$f(D|A,X,\omega) = \mathrm{tN}_D(AX', \omega^{-1}\Omega_p \otimes \Omega_n), \tag{2}$$

$$\Omega_p = \mathrm{diag}(D\mathbf{1}_{1,n}), \tag{3}$$

$$\Omega_n = \mathrm{diag}(\mathbf{1}_{1,p}D). \tag{4}$$

Here, diag(.) of vector argument composes square diagonal matrix with diagonal elements from its argument, $\mathbf{1}$ is a matrix of ones of dimensions given in its subscript, tN() denotes truncated normal density on positive support and $\otimes$ is the Kronecker product. Prior knowledge on the parameters is chosen as follows [10]:

$$f(A|\Upsilon) = \mathrm{tN}_A\left(\mathbf{0}_{p\times r}, \Omega_p \otimes \Upsilon^{-1}\right), \tag{5}$$

$$\Upsilon = \mathrm{diag}(v), v = [v_1,\ldots,v_r]',$$

$$f(v) = \prod_{i=1}^{r} G_{v_i}(\alpha_{i,0}, \beta_{i,0}), \tag{6}$$

$$f(X) = \mathrm{tN}_X\left(\mathbf{0}_{n,r}, \Omega_n \otimes I_r\right), \tag{7}$$

$$f(\omega) = G_\omega\left(\vartheta_0, \rho_0\right), \tag{8}$$

where I_p denotes the identity matrix of dimensions $p \times p$, $\Upsilon \in \mathbf{R}^{r\times r}$ is diagonal matrix with hyper-parameters v_i with prior statistics $\alpha_0, \beta_0 \in \mathbf{R}^r$, and $\vartheta_0, \rho_0 \in \mathbf{R}$ are scalar prior parameters. $G()$ denotes the Gamma distribution.

Truncation of (5) and (7) to positive values make this model distinct from the model of principal component analysis. For non-truncated priors (5) and (7) the variational algorithm converges to the solution given by the principal component analysis [10].

Product of densities (2)–(8) defines the joint likelihood that is approximated by the Variational Bayes method. The resulting approximate posterior marginals are found in the form [10]:

$$\tilde{f}(A|D,r) = \mathrm{tN}_A\left(\mu_A, \Omega_p \otimes \Sigma_A\right), \tag{9}$$

$$\tilde{f}(X|D,r) = \mathrm{tN}_X\left(\mu_X, \Omega_n \otimes \Sigma_X\right), \tag{10}$$

$$\tilde{f}(v|D,r) = \prod_{i=1}^{r} G_{v_i}\left(\alpha_i, \beta_i\right), \tag{11}$$

$$\tilde{f}(\omega|D,r) = G_\omega\left(\vartheta, \rho\right), \tag{12}$$

with shaping parameters:

$$\mu_A = \hat{\omega}\Omega_p D\Omega_n \widehat{X}\Sigma_A, \qquad \Sigma_A = \left(\hat{\omega}\widehat{X'\Omega_n X} + \widehat{\Upsilon}\right)^{-1},$$

$$\mu_X = \hat{\omega}\Omega_n D'\Omega_p \widehat{A}\Sigma_X, \qquad \Sigma_X = \left(\hat{\omega}\widehat{A'\Omega_p A} + I_r\right)^{-1},$$

$$\alpha = \alpha_0 + \frac{p}{2}\mathbf{1}_{r,1},$$

$$\beta = \beta_0 + \frac{1}{2}\,\mathrm{diag}\left(\widehat{A'\Omega_p A}\right),$$

$$\vartheta = \vartheta_0 + \frac{np}{2},$$

$$\rho = \rho_0 + \frac{1}{2}\,\mathrm{tr}\left(DD' - \widehat{A}\widehat{X}'D' - D\widehat{X}\widehat{A}'\right) + \frac{1}{2}\,\mathrm{tr}\left(\widehat{A'A}\widehat{X'X}\right).$$

Here, tr(.) denotes trace of its matrix argument.

The required moments are $\widehat{\Upsilon} = \mathrm{diag}(\alpha \circ \beta^{-1})$, where $\circ$ denotes the Hadamard product, $\widehat{\omega} = \vartheta/\rho$ and the moments of the truncated normal densities are computed with neglected covariances using relations in Appendix A.

2.2 Deconvolution

Deconvolution of factor curves is a well established method of curve analysis [6]. It is based on biologically-motivated assumptions that the time-activity curves of organs arise as convolution of the input activity (observed in the form of the curve of the blood) and organ-specific kernels. The shape of the kernels is expected to be formed by a constant plateau followed by monotonic decrease to zero, see Figure 1.

Formally, a single time-activity curve of the fth organ, x_f, can be modeled as

$$x_{t,f} = \sum_{m=1}^{t} b_{t-m+1}u_{m,f} \tag{13}$$

where b is the input activity curve, and u_f is the convolution kernel. For known x_f and b the convolution kernel u_f may be found by any deconvolution method. However, for inaccurate values of x_f and b, the result would not respect physiological assumptions in Figure 1. Therefore, [5] proposed to model the convolution kernel by a sum of non-negative increments:

$$u_{m,f} = \sum_{i=m}^{n} w_{i,f},\ w_{i,f} \geq 0. \tag{14}$$

Deconvolution under this assumption provides more physiologically meaningful results. However, the curves x_f and b still has to be known. We relax this restriction in the following Section.

3 Factor Analysis with Blind Deconvolution (CFA)

In this chapter, we combine method from chapters 2.1 and 2.2. The likelihood function (2) as well as the prior densi-

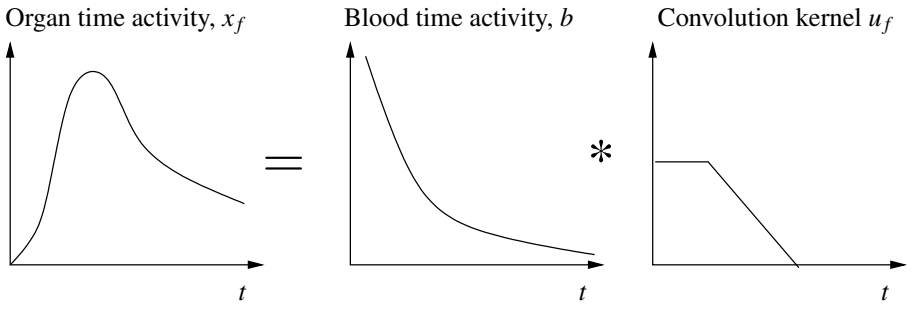

Figure 1. Illustration of the assumed shape of the convolution kernels.

ties (5), (6), (8) are modified by substitution

$$X = BCW, \tag{15}$$

where B is a matrix composed of the blood vector b, and C is an auxiliary function:

$$B = \begin{bmatrix} b_1 & 0 & \cdots & 0 \\ b_2 & b_1 & \ddots & \vdots \\ \vdots & \ddots & \ddots & 0 \\ b_n & \cdots & b_2 & b_1 \end{bmatrix}, \quad C = \begin{bmatrix} 1 & 1 & \cdots & 1 \\ 0 & 1 & \ddots & \vdots \\ \vdots & \ddots & \ddots & 1 \\ 0 & \cdots & 0 & 1 \end{bmatrix}.$$

Each b and W have additional constraints modeled in a probabilistic way.

3.1 Model of the blood curve

Due to radioactive decay and physiological processes, the time-activity curve of the blood is assumed to be non-negative. Therefore, we define b as a sum of non-negative increments:

$$b_t = \sum_{i=t}^{n} g_i, \; g_i \geq 0. \tag{16}$$

The unknown variable is then g with prior density

$$f(g|\psi) = \mathrm{tN}(\mathbf{0}_n, \psi^{-1} I_n), \tag{17}$$
$$f(\psi) = G_\psi(\zeta_0, \eta_0) \tag{18}$$

where ψ is a hyper-parameter of the variance with scalar prior parameters ζ_0 and η_0. The assumption of non-negative elements of g is again modeled by a truncated Gaussian (17). Validity of this assumption will be discussed in Section 5.

3.2 Model of impulse retention functions

Assumption on the convolution kernel U, Figure 1, transforms the assumptions on W to two parts, Figure 2:

$$w_{i,f} = \begin{cases} h_f & s_f \leq i \leq s_f + l_f, \\ 0 & \text{otherwise.} \end{cases} \tag{19}$$

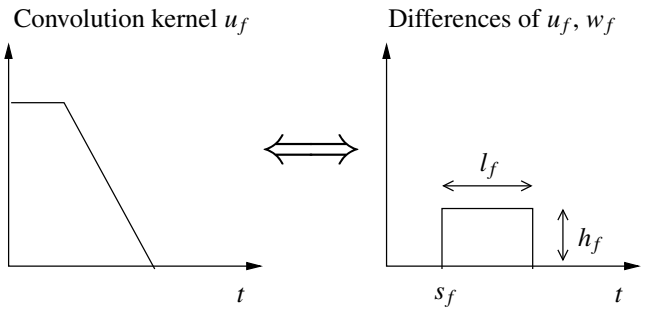

Figure 2. Parametrization of the convolution kernel via differences

Here, s_f denotes beginning of the slope on the convolution kernel, l_f is the length of the slope, and h_f is a parameter of steepness of the slope. All of these parameters are unknown with prior distribution chosen as

$$f(h) = tN(0_{r,1}, \tau_0 I_r), \tag{20}$$
$$f(s_i) = U(0,n), \quad \forall i \in \{1,\ldots,r\}, \tag{21}$$
$$f(l_i|s_i) = U(0,n-s_i), \quad \forall i \in \{1,\ldots,r\}, \tag{22}$$

where τ_0 is a prior scalar parameter.

We consider model (19) only as our prior knowledge, from which the real curves can depart. Therefore, (19) models only mean value of the prior distribution on W:

$$f(W|\Xi) = \mathrm{tN}(M_W, I_n \otimes \Xi_W^{-1}), \; \Xi_W = \mathrm{diag}(\xi_1,\ldots,\xi_r), \tag{23}$$

$$f(\xi_f) = G_{\xi_f}(\kappa_{f,0}, \nu_{f,0}), \tag{24}$$

where $M_W = [m_{w1},\ldots,m_{w,r}]$, $m_{w,f} = [0,\ldots,h_f,\ldots h_f,0\ldots 0]$. Strictness of the requirement that W would be close to M_W is governed by prior variance Ξ_W. The variance is also unknown, hyper-parameterized by ξ_f with scalar prior parameters $\kappa_{f,0}$ and $\nu_{f,0}$.

3.3 Variational Solution

Joint likelihood for new model is obtained by replacing (7) in Section 2.1 with prior information (17)–(24). Follow-

ing the Variational Bayes method we identify the following approximate posterior distributions:

$$\begin{aligned}
\tilde{f}(A|D,r) &= N_A(\mu_A, \Omega_p^{-1} \otimes \Phi_A),\\
\tilde{f}(g|D,r) &= N_g(\mu_g, \Sigma_g),\\
\tilde{f}(\mathrm{vec}(W)|D,r) &= N_{\mathrm{vec}(W)}(\mu_{\mathrm{vec}(W)}, \Sigma_{\mathrm{vec}(W)}),\\
\tilde{f}(v|D,r) &= \prod_{i=1}^{r} G_{v_i}(\alpha_i, \beta_i),\\
\tilde{f}(\mathrm{diag}(\Xi_W)|D,r) &= \prod_{i=1}^{r} G_{\xi_i}(\kappa_i, \nu_i),\\
\tilde{f}(\psi|D,r) &= G_{\psi}(\zeta, \eta),\\
\tilde{f}(\omega|D,r) &= G_{\omega}(\vartheta, \rho),
\end{aligned}$$

where diag(.) of matrix argument denotes vector composed of diagonal entries of the matrix, vec(.) of matrix argument denotes vector composed of its columns. Shaping parameters are:

$$\begin{aligned}
\Phi_A &= (\widehat{\omega}\widehat{X'\Omega_n X} + \widehat{\Upsilon})^{-1},\\
\mu_A &= \Omega_p^{-1}(\widehat{\omega}\Omega_p D \Omega_n \widehat{X})\Phi_A,\\
\Sigma_g &= (\widehat{\psi} I_n + C' \sum_{i,j=1}^{r} Z_{i,j} C)^{-1},\\
Z_{i,j} &= \widehat{a_i'\Omega_p a_j} \sum_{k,l=0}^{n-1} \Delta_k' \Delta_l \widehat{\Omega_n}(u_{k+1,j}\widehat{u_{l+1,i}}),\\
\mu_g &= \Sigma_g C' \sum_{i=1}^{r} \left(\left(\sum_{k=0}^{n-1} \Delta_k' \widehat{u_{k+1,i}} \right) \Omega_n D' \Omega_p \widehat{a_i} \right),\\
\Sigma_{\mathrm{vec}(W)} &= \left(((\widehat{A'\Omega_p A})' \otimes \widehat{\omega} C' \widehat{B'\Omega_n B} C) + (\widehat{\Xi_W} \otimes I_n) \right)^{-1},\\
\mu_{\mathrm{vec}(W)} &= \Sigma_{\mathrm{vec}(W)} \left(\Sigma_{ABC}\, \mathrm{vec}(\mu_W^{(1)}) + (\widehat{\Xi_W} \otimes I_n)\, \mathrm{vec}(\widehat{M_W}) \right),\\
\Sigma_{ABC} &= \left((\widehat{A'\Omega_p A})' \otimes \widehat{\omega} C' \widehat{B'\Omega_n B} C \right)\\
\mu_W^{(1)} &= (C'\widehat{B'\Omega_n B}C)^{-1} C' \widehat{B}' \Omega_n D' \Omega_p \widehat{A} (\widehat{A'\Omega_p A})^{-1},
\end{aligned}$$

$$\begin{aligned}
\alpha &= \alpha_0 + \frac{p}{2}\mathbf{1}_{r,1}, \quad & \beta &= \beta_0 + \frac{1}{2}\mathrm{diag}(\widehat{A'A}),\\
\kappa &= \kappa_0 + \frac{n}{2}\mathbf{1}_{r,1}, \quad & \nu &= \nu_0 + \frac{1}{2}\mathrm{diag}(\widehat{W'W})\\
& & & \quad + \frac{1}{2}\mathrm{diag}(-2\widehat{W}'\widehat{M_W}) + \frac{1}{2}\mathrm{diag}(\widehat{M_W'M_W}),\\
\zeta &= \zeta_0 + \frac{n}{2}, & \eta &= \eta_0 + \frac{1}{2}\mathrm{tr}(\widehat{g'g}),\\
\vartheta &= \vartheta_0 + \frac{np}{2}, & \rho &= \rho_0 + \frac{1}{2}\mathrm{tr}(\Omega_p D \Omega_n D' - 2\Omega_p \widehat{A}\widehat{X}'\Omega_n D')\\
& & & \quad + \frac{1}{2}\mathrm{tr}\left(E_{f(A|D,r)}(A\widehat{X'\Omega_n X}A') \right),
\end{aligned}$$

where auxiliary matrix $\Delta_k \in \mathbf{R}^{n\times n}$ is defined as $(\Delta_k)_{i,j} = \begin{cases} 1 & i-j=k \\ 0 & otherwise \end{cases}$ and a_j denotes the jth column of matrix A.

The required moments are $\widehat{\Upsilon} = \mathrm{diag}(\alpha \circ \beta^{-1})$, $\widehat{\omega} = \vartheta/\rho$, $\Xi_W = \mathrm{diag}(\kappa \circ \nu^{-1})$, $\psi = \zeta/\eta$ and the moments of the truncated normal densities are computed with neglected covariances using relations in Appendix A.

4 Experiments with clinical data

Performance of the proposed algorithm was compared to that of the traditional two-step approach on sets of scintigraphic images of renal activity. Three different sets were selected for illustration: one set is physiological (IM3) and two are harmed (IM1 and IM2), see Table 1.

4.1 Estimation of convolution kernel using FA and CFA

Assumptions listed in Section 3.2 are valid in the so-called uptake part of a renal scintigraphic sequence. Results of analysis of one such sequence are displayed in Figure 3 for two methods: CFA (Section 3) at the top, and the two step approach using FA (Section 2.1) followed by deconvolution (Section 2.2) at the bottom. Specifically, time activity curves corresponding to two factors—tissue background and blood stream—are displayed in tandem with their estimated convolution kernel in the same order as in Figure 1. For both methods, the estimates of the time activity curves are displayed in the form of posterior mean values, i.e. $\widehat{X}$. Two curves of the convolution kernel for the CFA correspond to the hyper-parameter M_W transformed into the space of U (dashed line) and posterior estimate of U (solid line). In the FA case, the convolution kernel is computed from the blood curve and the tissue background curve using Fourier transform.

Note that the time activity curve of the background tissue obtained from the FA method is not smooth, yielding unrealistic convolution kernel. For this particular data set, the result heavily depends on the chosen number of factors, r. The presented results are obtained for $r = 3$. For higher number of factors, the activity in background tissues is split into several factors, rendering deconvolution unreliable. The CFA method is less sensitive to this choice since the assumption of common convolution kernel results in smoother estimates of the curves and the convolution kernels. Consequently, the CFA method aggregates more activity in the background factor. This behavior is significant for analysis of relative function of the kidneys.

4.2 Analysis of relative kidney function

Relative function of kidneys is evaluated using the renal clearance of a kidney defined by $rel_L = \frac{L}{R+L} \times 100$, where L and R denotes intensity of left and right parenchyma. The analysis is typically performed by an expert using a set of tools including FA and deconvolution. The first step of such analysis is to identify the regions of interest for

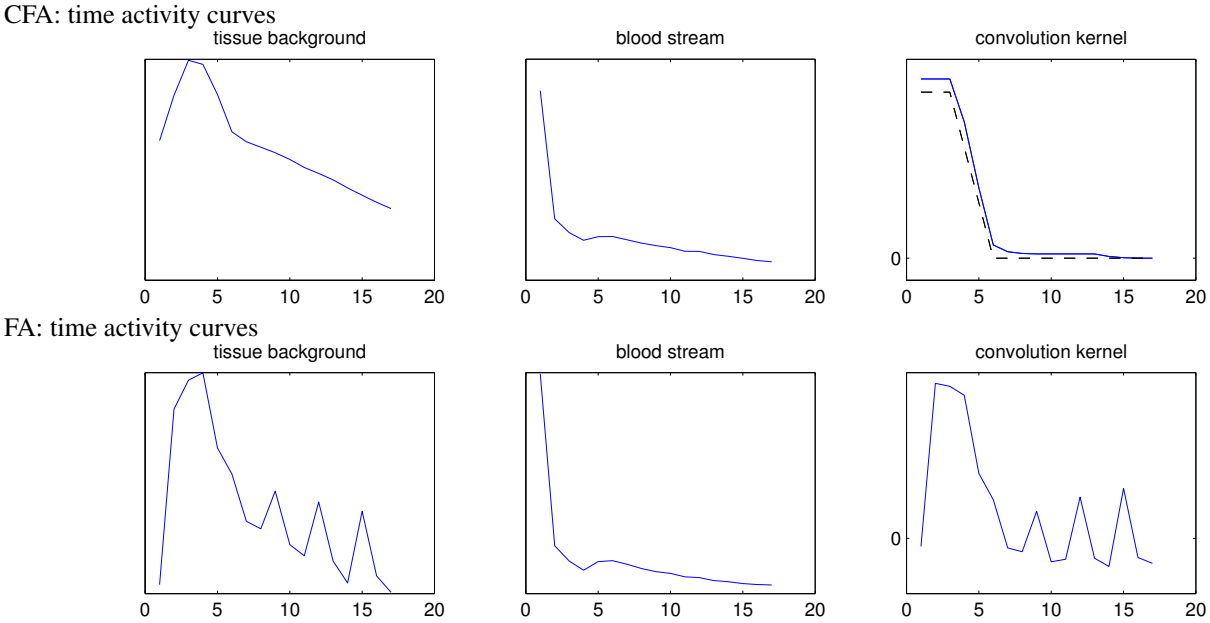

Figure 3. Time-activity curves of tissue background, blood stream and their estimated convolution kernel are displayed in the same order as in Figure 1.

each kidney. In our experiment, rectangular regions of interest were manually positioned around the kidneys and the proposed algorithm was run in each of them. For comparison, the original factor analysis without the convolution modeling was also performed. Factors corresponding to the parenchyma were identified manually and total activity of the each parenchyma, L and R, was computed. The resulting relative function rel_L was compared to that obtained by an expert using manually drawn regions-of-interest of the parenchyma with hand tuned subtraction of the background tissue activity.

Comparison of all three approaches on three sets of clinical data is summarized in Table 1. We note that for healthy organs (IM3), both variants of the factor analysis provide comparable results which correspond to the expert chosen values. However, CFA outperforms FA in separation of the background from the parenchyma in pathological cases (IM1 and IM2). Detailed analysis of the IM2 data set is displayed in Figure 4. Note that factor images (variable A) are almost identical for both cases, the main difference is in the proportion of time activity curves, Figure 4, middle right and right column. Specifically, the estimates of the background tissue activity produced by CFA are much higher that that of FA, which significantly impacts evaluation of the relative renal clearance.

data set	expert	FA	CFA
IM1	28%–31%	34%	29%
IM2	69%–76%	93%	75%
IM3	48%–51%	48%	49%

Table 1. Comparison of estimates of relative function of the left kidney obtained by expert solution and semi-automatic methods.

5 Discussion

The results presented in Section 4 suggest that the factor analysis with integrated model of convolution of factor curves has potential to improve estimation of organ activity. However, the methods is still not ready for routine use. This may be either due to the use of inappropriate assumptions or due to the approximations made in evaluation for the posterior. We discuss some potential issues and ways to improve them.

Modeling of the blood curve by increments (16) was motivated by the assumption that the activity in the blood is monotonically decreasing in time. However, variants of the resulting algorithm with enforced positivity of increments g performed worse that those without this restriction. Without enforced positivity of g, the occurrence of negative values in the estimate was rather sparse. We conjecture that this is due to the fact that we observe only a fraction of the blood activity in the selected region of interest. From this point of view, g is an arbitrary parameter and may be removed in future versions of the model.

The assumption of common variances of differences on the whole curve, ξ_f in (23), was motivated by computational reasons. It was found to be rather strict. As a consequence of this assumption the estimates of prior mean values of the convolution kernels were sharply peaked and unrealistic. More detailed modeling of variances Ξ in (12) would be necessary for improvement.

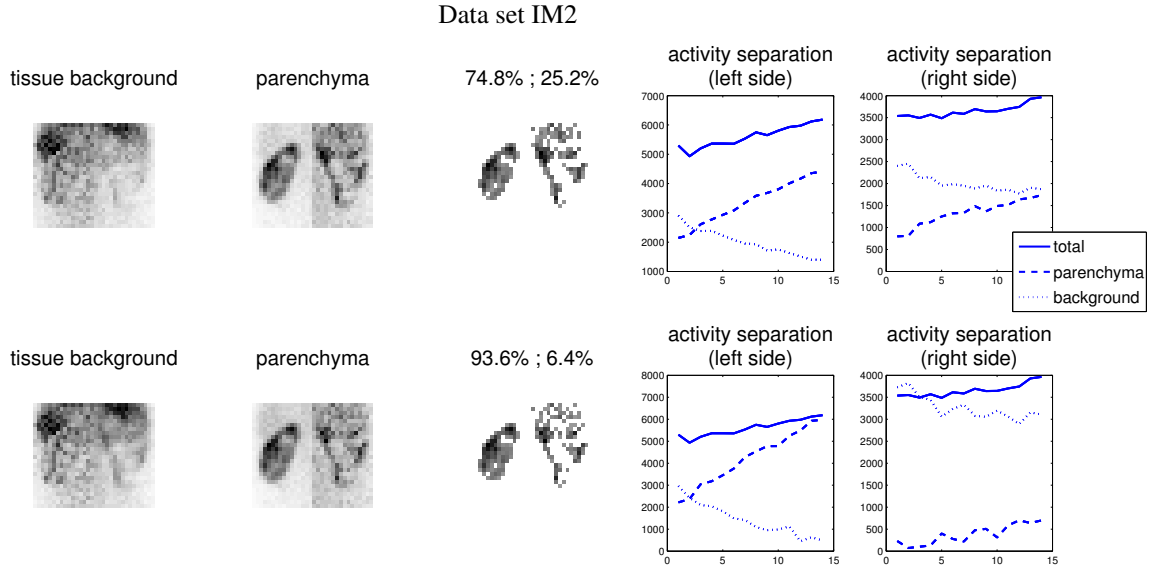

Figure 4. Relative function of kidneys for data set IM2 obtained from CFA (top row) and FA (bottom row). Left: estimates of the background tissue activity. Middle-left: estimates of the parenchyma activity. Middle: thresholded pictures of the parenchyma used for evaluation of the relative function. Middle-right: separation of total activity in the left region into those of background tissue and parenchyma. Right: separation of total activity in the right region into those of background tissue and parenchyma.

Assumptions similar to (19) can be used for automatic estimation of regions of interest in the factor images. Preliminary experiments reveal the same need for finer modeling of its prior covariance that in the case of Ξ. Success in this direction would allow completely automatic selection of regions of interest without the need for manual selection of left and right kidney.

6 Conclusion

A new mathematical model for functional analysis of dynamic scintigraphic images is proposed. The key novelty of the model is parametrization of the factor curves by convolution of a common input activity with organ specific convolution kernels. The convolution kernels are restricted according to physiological assumptions. Estimates of the model parameters are obtained using the Variational Bayesian estimation procedure. The methodology is flexible enough to allow addition of other physiologically meaningful assumptions and obtain different estimation algorithms. The model was tested on clinical data from renal scintigraphy where improvement over previous methods was demonstrated especially on demanding data sets.

Acknowledgement

Support of grant GA CR 303/07/0950 is gratefully acknowledged.

A Moments of truncated Normal Distribution

Scalar truncated normal distribution

$$tN_x(x|\mu,r) = \alpha\sqrt{2}\exp(-(x-\mu)^2/(2r)),\ x>0, \quad (25)$$

has moments

$$\widehat{x} = \mu + r\alpha\sqrt{2}\exp(-\mu^2/(2r)), \quad \widehat{x^2} = r + \mu\widehat{x},$$

where $\alpha^{-1} = \sqrt{\pi r}(1-\mathrm{erf}(-\mu/\sqrt{2r}))$ and erf is the error function.

References

[1] Buvat, I., Benali, H., Di Paola, R.: Statistical distribution of factors and factor images in factor analysis of medical image sequences. Physics in Medicine and Biology 43(6), 1695–1711 (1998)

[2] Durand, E., Blaufox, M., Britton, K., Carlsen, O., Cosgriff, P., Fine, E., Fleming, J., Nimmon, C., Piepsz, A., Prigent, A., et al.: International Scientific Committee of Radionuclides in Nephrourology (ISCORN) consensus on renal transit time measurements. In: Seminars in nuclear medicine. vol. 38, pp. 82–102. Elsevier (2008)

[3] Fine, J., Pouse, A.: Asymptotic study of the multivariate functional model. application to the metric of choise in principal component analysis. Statistics 23, 63–83 (1992)

[4] Klein, R., Beanlands, R., Adler, A., deKemp, R.: Model-based factor analysis of dynamic sequences of cardiac positron emission tomography. In: Nuclear Science Symposium Conference Record, 2008. NSS'08. IEEE. pp. 5198–5202. IEEE (2009)

[5] Kuruc, A., Caldicott, W., Treves, S.: An improved deconvolution technique for the calculation of renal retention functions. Computers and Biomedical Research 15(1), 46–56 (1982)

[6] Lawson, R.: Application of mathematical methods in dynamic nuclear medicine studies. Physics in medicine and biology 44, R57 (1999)

[7] Lueck, G., Kim, T., Burns, P., Martel, A.: Hepatic perfusion imaging using factor analysis of contrast enhanced ultrasound. Medical Imaging, IEEE Transactions on 27(10), 1449–1457 (2008)

[8] Miskin, J.W.: Ensemble Learning for Independent Component Analysis. Ph.D. thesis, University of Cambridge (2000)

[9] Molina, R., Mateos, J., Katsaggelos, A.: Blind deconvolution using a variational approach to parameter, image, and blur estimation. Image Processing, IEEE Transactions on 15(12), 3715–3727 (2006)

[10] Šmídl, V., Quinn, A.: The Variational Bayes Method in Signal Processing. Springer (2005)

[11] Šámal, M., Kárný, M., Sůrová, H., Maříková, E., Dienstbier, Z.: Rotation to simple structure in factor analysis of dynamic radionuclide studies. Physics in Medicine and Biology 32, 371–382 (1987)

[12] Šámal, M., Kárný, M., Sůrová, H., Pěnička, P., Maříková, E., Dienstbier, Z.: On existence of unambiguous solution in factor analysis of dynamic studies. Physics in Medicine and Biology 34, 223–228 (1989)